JOURNAL OF MATERIALS SCIENCE **35** (2000) 1105–1113

Quantitative phase analysis by X-ray diffraction of martensite and austenite in strongly oriented orthodontic stainless steel wires

R. W. CHEARY
Department of Applied Physics, University of Technology Sydney, NSW 2007, Australia
E-mail: cheary@phys.uts.edu.au

YING MA-SORRELL
Key Centre for Microscopy & Microanalysis and Faculty of Dentistry, University of Sydney, NSW 2006, Australia

A method is described for measuring the volume fractions and textures of martensite and austenite in strongly textured stainless steel orthodontic wires using a conventional X-ray diffractometer. These wires display a classic fibre texture with the ⟨111⟩ of the FCC austenite phase and the ⟨110⟩ of the BCC martensite phase aligned parallel to the wire axis. The samples analysed consisted of wire cross-sections bundled together and chemically polished in an epoxy disc. In this form the dominant lines in the XRD patterns are the austenite (111) and the martensite (110). On the basis of X-ray diffraction results from these two lines only, procedures are described for, (a) correcting the X-ray intensity data for both the finite size and irregular cross-sectional shape of the specimens in relation to the X-ray beam footprint, (b) separately measuring the texture of the austenite and martensite phases and, (c) correcting the 111 and 110 integrated intensities for texture. These procedures are illustrated using X-ray data from four different orthodontic wires. The factors limiting the accuracy of the phase analysis are discussed.

1. Introduction

AISI 302 type stainless steels were introduced as orthodontic wires in 1929 [1, 2]. Since then they have been the primary alloys for orthodontic wires. They have strength, a high modulus of elasticity, excellent formability, good corrosion resistance, and are available at a moderate cost [3, 4]. The mechanical properties of orthodontic wires are governed primarily by their microstructure and one of the main factors controlling this is the forming process. Type 302 orthodontic wires are produced by a cold drawing process combined with intermediate annealing heat treatments. Although the basic atomic arrangement of 302 stainless steel is face centred cubic austenite, partial transformation to alpha or epsilon martensite, occurs during the drawing of the wire owing to the large deformation associated with this process [5, 6]. One of the benefits of the stress-induced transformation of austenite to martensite is the increase in strength of orthodontic wires. For clinical applications, therefore, it is important to be able to measure and control the relative proportions of austenite and martensite in order to optimise and identify the conditions for high strength without loss of ductility.

The work presented in this paper on the quantification of martensite and austenite in orthodontic wires by X-ray diffraction (XRD), is part of a broader investigation of the mechanical and microstructural properties of these wires. XRD is a well established technique for quantifying the martensite and austenite [7, 8] because the peaks from these phases are easily resolved even in heavily deformed and fined grained materials used in the present investigation (see Fig. 1). Provided the crystallites in the material are randomly oriented or nearly randomly orientated, it is a relatively simple matter to quantify the phase content of the wires through an analysis of the integrated intensities of the diffraction peaks. However, orthodontic wires generally have a strong texture and the conventional quantitative XRD intensity relations based on randomly oriented crystals are invalid. Accordingly, we have developed a method for determining the austenite and martensite phase content even when a strong texture exists in wires. This is based on measuring the integrated intensities of 110-martensite and 111-austenite lines, and the preferred orientation distribution from wire cross sections using a conventional diffractometer. Analytical procedures are described for coping with the preferred orientation and the irregular finite lateral dimensions of the wire specimens.

2. Measurement theory & experimental technique

These investigations were carried out on two different brands of orthodontic wire, referred to here as Type

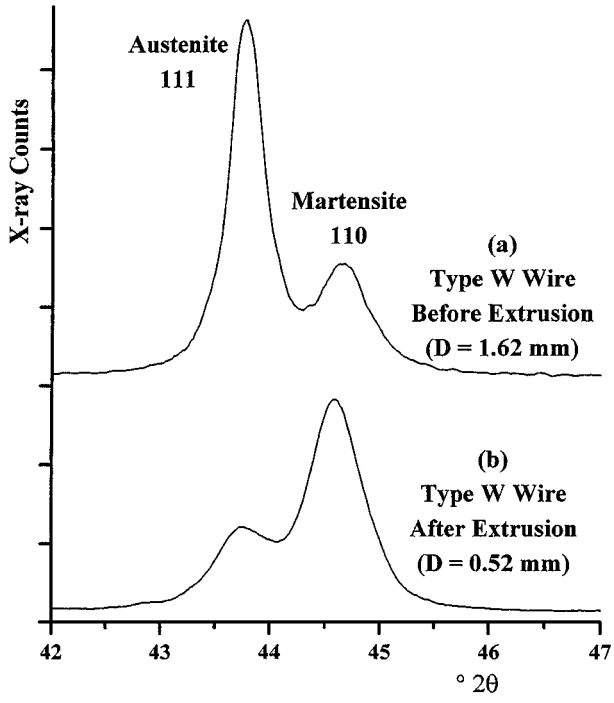

Figure 1 111 Austenite and 110 martensite profiles from two orthodontic wires, (a) before extrusion ($D = 1.62$ mm) and (b) after extrusion ($D = 0.52$ mm). A large proportion of the austenite is transformed into martensite during the extrusion process.

W and Type D, which are manufactured in different countries;

- Type W Wires. These have diameters of 0.52 mm and 1.62 mm. The 0.52 mm diameter wire is the one used in orthodontic applications. The 1.62 diameter wire is the starting material before extrusion to form the 0.52 mm diameter wire.
- Type D Wires. These have diameters of 0.88 mm and 2.18 mm. The 0.88 mm diameter wire is the one used in orthodontic practice. The 2.18 mm diameter wire is the starting material before extrusion to form the 0.88 mm diameter wire.

These wires contain the γ-austenitic and α-martensitic phases. Other phases that are known to occur in orthodontic wires, such as δ-ferrite (δ-Fe), chromium carbide ($Cr_{23}C_6$, Cr_7C_3) and iron carbide (Fe_3C), were not observed.

According to [7], the integrated intensities of the martensite and austenite diffraction lines, I_{M}^{hkl} and I_{A}^{HKL}, are given in terms of the volume fractions V_{M} and V_{A} $(= 1 - V_{\mathrm{M}})$ of each phase by,

$$I_{\mathrm{M}}^{hkl} = \frac{C V_{\mathrm{M}} m_{hkl} \mathrm{LP}(\theta_{\mathrm{M}}) F_{\mathrm{M}}^2 e^{-B_{\mathrm{M}}/2d_{\mathrm{M}}^2}}{v_{\mathrm{M}}^2}$$

and

$$I_{\mathrm{A}}^{HKL} = \frac{C V_{\mathrm{A}} m_{HKL} \mathrm{LP}(\theta_{\mathrm{A}}) F_{\mathrm{A}}^2 e^{-B_{\mathrm{A}}/2d_{\mathrm{A}}^2}}{v_{\mathrm{A}}^2} \qquad (1)$$

where, C is a constant embodying the dimensions of the diffractometer, the incident beam power and the attenuation coefficient μ of the sample (it is assumed that $\mu_{\mathrm{M}} = \mu_{\mathrm{A}}$), m_{hkl} and m_{HKL} are the multiplicity factors, v_{M} and v_{A} are the cell volumes, d_{M} and d_{A} are the d spacings in martensite and austenite, respectively, F_{M} and F_{A} are the structure factors for the hkl and HKL lines respectively, B_{M} and B_{A} are the Debye-Waller factors for each phase, LP (θ_{M}) and LP (θ_{A}) are the Lorentz-Polarization factors which, for the diffractometer used in this work, are given by $\mathrm{LP}(\theta) = (1 + \cos^2 2\theta \cos^2 2\theta_{\mathrm{mono}})/\sin 2\theta \cos\theta$ where θ_{mono} is the Bragg angle of the graphite diffracted beam monochromator (i.e. $\theta_{\mathrm{mono}} = 13.3^\circ$). To simplify the analysis, the Equation 1 may be abbreviated to

$$I_{\mathrm{M}}^{hkl} = C m_{hkl} V_{\mathrm{M}} K_{\mathrm{M}}^{hkl}$$

and

$$I_{\mathrm{A}}^{HKL} = C m_{HKL} V_{\mathrm{A}} K_{\mathrm{A}}^{HKL} \qquad (2)$$

where K_{M}^{hkl} and K_{A}^{HKL} contain terms such as the structure factor and cell volume that can be calculated from the known structures of the two phases. In principle, therefore, by measuring the integrated intensities of any two lines in orthodontic steel, the volume fraction (or mass fraction) of either the martensite or austenite phases can be determined from,

$$\frac{I_{\mathrm{M}}^{hkl}}{I_{\mathrm{A}}^{HKL}} = \frac{V_{\mathrm{M}}}{(1 - V_{\mathrm{M}})} \frac{K_{\mathrm{M}}^{hkl}}{K_{\mathrm{A}}^{hkl}} \frac{m_{hkl}}{m_{HKL}} \qquad (3)$$

In the present samples both phases displayed strong textures along the axis of the wires corresponding to austenite [111] and martensite [110]. For very narrow wires the degree of preferred orientation during manufacture is often so strong that only the 111-austenite line and the 110-martensite line can be observed in diffractometer patterns taken of wire cross-sections. In such circumstances, accurate quantitative analysis based on the random crystal model, represented by Equation 1, cannot be carried out without a large correction for preferred orientation. However, when the orientation distributions of the two phases are similar the preferred orientation corrections will also be similar and Equation 3 is still valid for semi-quantitative analysis if used with the appropriate pair of lines. Such a pair is the 111-austenite line and the 110-martensite lines because the stress induced phase transformation results in the 111 austenite plane converting into a 110 martensite plane. Although there is an orientation change during transformation, the actual orientation distributions of the 111 austenite and 110 martensite planes will be approximately the same although the martensite orientation distribution is expected to be a few degrees broader. For accurate quantitative analysis however, allowance should be made for any differences in the orientation distribution of the two phases. This is the approach adopted in the present investigation.

All the XRD data were collected by reflection diffraction using a conventional Siemens D5000 diffractometer with a graphite diffracted beam monochromator. Two forms of sample were prepared by embedding wires in an epoxy resin composite and then chemically polishing the exposed wires to obtain a smooth undamaged surface. Illustrations of the two types of sample

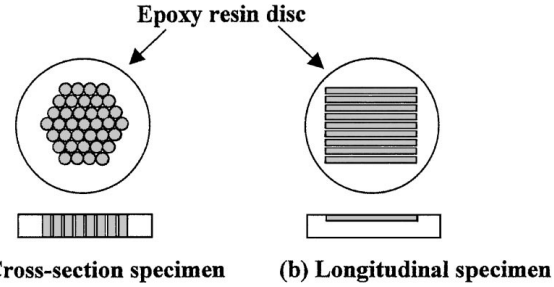

Figure 2 Types of specimens prepared for XRD analysis to measure the martensite/austenite content in orthodontic stainless steels.

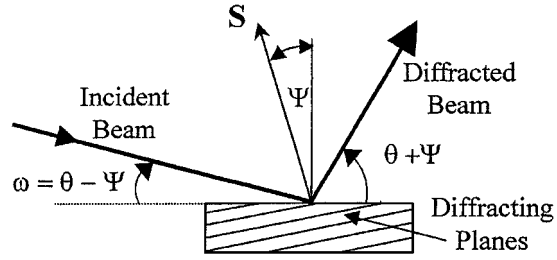

Figure 3 Asymmetric diffraction to measure the intensity diffracted from *hkl* planes at an angle ψ to the surface of the specimen.

are shown in Fig. 2. After a preliminary investigation of the XRD patterns and the results from each type of specimen, it was decided to use only cross-section specimens shown in Fig. 2a.

In specimens of type (a) the austenite 111 line is much more intense than the same line in type (b) specimens whereas the martensite 110 line is approximately the same intensity in both specimen types. This arises because the normals to the 111 austenite and 110 martensite planes are strongly orientated along the axes of the wires. Given this condition then other members of the austenite {111} family will be centred about angles of 70.5°, 109.5° and 180° with respect to the axis of the wire. There are fewer crystals therefore oriented with any of the {111} family at 90° to the wire axis. Alternatively, for every 110 plane oriented along the wire axis there will be other members of the {110} family at 90° and 180°. Hence the 110 martensite line tends to be equally intense in both longitudinal and cross-section specimens. On the whole, cross-sectional specimens of type (a) give the strongest combination of 111 austenite and 110 martensite lines and are easier to interpret because of the well-defined and reproducible nature of the preferred orientation. As the intensity of lines other than the 110 martensite and the 111 austenite can be very small, all the quantitative analysis has been done using the integrated intensities of these two lines only. Fortunately these lines can be measured with good precision which is particularly important for measuring the preferred orientation distribution where the diffractometer is set-up in an asymmetric condition thereby causing defocussing and diminished intensities.

The procedure developed here for correcting the observed integrated intensities for preferred orientation depends on being able to determine the preferred orientation distributions of the austenite and martensite phases in the wires. A unique aspect of the present procedure is the development of a correction mechanism that not only compensates for the preferred orientation, but also for the finite size and slightly irregular areal shape of the specimens.

As the specimens are always set spinning about an axis perpendicular to the specimen surface, the preferred orientation distribution of each phase will depend only on the angle ψ between the normal to the specimen (i.e. the wire axis) and the normals to the hkl planes. The orientation distribution can be derived by carrying out asymmetric diffraction so that crystals with their planes oriented at an angle ψ to the surface normal come into the diffraction condition [9–11]. In the present samples asymmetric diffraction has been used to determine the integrated intensities, $I_{\mathrm{M}}^{110}(\psi)$ and $I_{\mathrm{A}}^{111}(\psi)$, of the 110 martensite and 111 austenite lines as function of the off-set angle ψ between the normal to the specimen and the diffraction vector **S** as shown in Fig. 3.

Under the asymmetric diffraction conditions shown in Fig. 3, diffraction profiles from a conventional diffractometer are defocussed and broaden with increasing ψ, particularly at low 2θ angles. An example of the 110 martensite and 111 austenite diffraction profiles obtained from one of the orthodontic wires for a range of off-set angles ψ from 0° up to 12° is shown in Fig. 4. Owing to the high concentration of dislocations in the wires, the diffraction lines were very broad (FWHM $\approx 0.5°$ or more) and the defocussing and instrumental broadening was overshadowed by the specimen diffraction broadening. All the measured X-ray profiles $D(2\theta)$ were symmetric and could be accurately fitted by representing each emission line in the Cu K_α spectrum with a pseudo-Voigt function [12], i.e.

$$D(2\theta) = \gamma L(2\theta) + (1-\gamma)G(2\theta) \qquad (4)$$

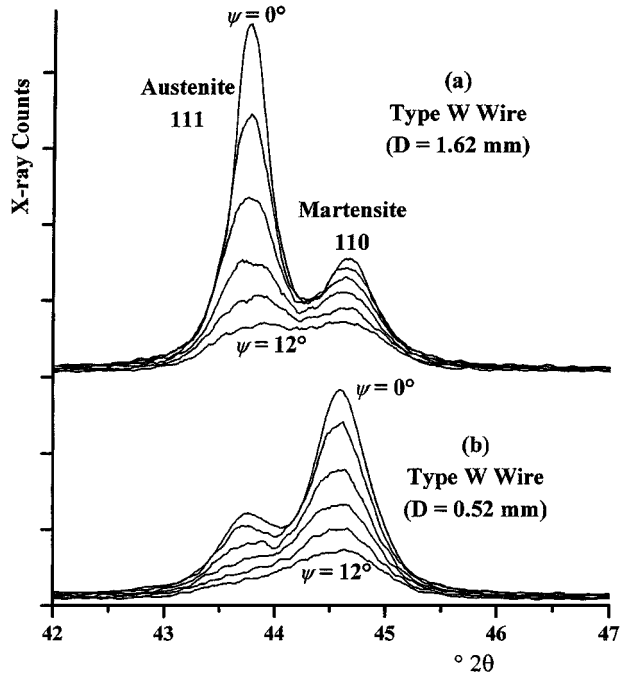

Figure 4 The 110 martensite and 111 austenite lines from an orthodontic wire recorded at different offset angles ψ between 0° and 12° at steps of 2°. The plot for $\psi = 2°$ is omitted for clarity as the profile is almost the same as for $\psi = 0°$.

where $L(2\theta)$ = Lorentzian function and $G(2\theta)$ = Gaussian function. All the integrated intensities, $I_M^{110}(\psi)$ and $I_A^{111}(\psi)$, were therefore determined from profile fitting using the X-ray software package XFIT [13, 14].

In specimens with random crystallites the integrated intensity $I_X(\psi)$ of the line from phase X (i.e. X = A or M) varies with the off-set angle ψ as

$$I_X(\psi) = I_X^{hkl}(1 + \tan\psi \cot\theta) \quad (5)$$

where I_X^{hkl} is the integrated intensity obtained under symmetric diffraction conditions at $\psi = 0^\circ$ for the hkl line in phase X for random crystals. This variation with ψ arises from changes in X-ray absorption and beam spread W across the sample surface when the X-ray beam is incident at an angle ω which is different from the Bragg angle θ (see Fig. 5). In the present samples the crystallites in the wires are not randomly oriented. Also, the specimens have a finite lateral size so that the incident beam can extend beyond the specimen, as illustrated in Fig. 5, giving a reduced integrated intensity relative to an "infinite" specimen. Under these circumstances Equation 5 for phase X has to be modified to,

$$I_X(\psi) = f(W)P_X(\psi)I_X^{hkl}(1 + \tan\psi \cot\theta) \quad (6)$$

where, $f(W)$ represents the fraction of the beam's footprint incident on the specimen when the beamspread is W and, $P_X(\psi)$ is the ratio of the number of crystallites oriented in the direction of the diffraction vector **S** relative to the random crystal model.

To apply Equation 6, it is necessary to determine $f(W)$ for each specimen. The effect on the integrated intensity of the incident beam spreading across and beyond the limits of the sample can be characterised by measuring the integrated intensity $I(\alpha)$ of a profile as a function of the angle of divergence α. At any divergence angle α, the beamwidth W is given by the relation,

$$W = \frac{\alpha R \operatorname{cosec}\omega}{1 - (\alpha/2)^2 \cot^2\omega} \quad (7)$$

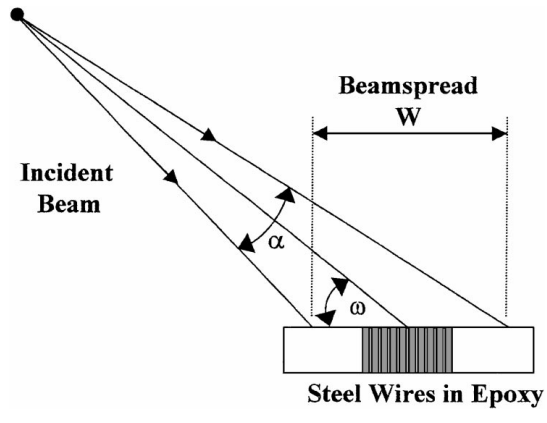

Figure 5 Spread W of the incident beam across a specimen surface for a diffractometer, of radius R, set at an equatorial divergence α and an incident angle ω.

where ω is the angle of incidence and R is the radius of the diffractometer. At small α, when the beam is contained within the specimen, the integrated intensity $I(\alpha)$ increases linearly with α. For an infinite specimen $I(\alpha)$ would continue to increase linearly with α and it is this line that defines $f(W) = 1$. For a finite specimen the rate of increase of $I(\alpha)$ with α will decrease and then flatten off as the beam spreads beyond the limits of the diffracting sample. Provided the region over which $f(W) = 1$ is sufficiently long to clearly identify the linear region in $I(\alpha)$ then, by extrapolating the linear portion of $I(\alpha)$ to large α to identify $I(\alpha)_{\text{extrap}}$, the correction factor $f(W)$ is given by,

$$f(W) = \frac{I(\alpha)_{\text{measured}}}{I(\alpha)_{\text{extrap}}} \quad (8)$$

In the present work, $f(W)$ was measured separately for each of the four wire specimens using a Siemens D5000 X-ray diffractometer operating in a symmetric mode (i.e. $\omega = \theta$) with the sample spinning and fitted with stepper motor controlled divergence slits which can be automatically incremented in steps of 0.1° from 0.2° up to 3°. Either the 111 austenite or the 110 martensite profile was measured at each α to determine $I(\alpha)$ depending on which line was stronger. An illustration of the results obtained for one of the wires is given in Fig. 6a, but with α converted to W using Equation 7 to obtain the variation in the integrated intensity $I(W)$ with beamspead W, and the expected variation $I(W)_{\text{extrap}}$ for an infinite specimen. Fig. 6b shows the form of $f(W)$, determined from $I(W)$ and $I(W)_{\text{extrap}}$, which for convenience was fitted with a sixth order polynomial. During the determination of $f(W)$ the divergence angle α is a variable term and ω is fixed at θ. When the diffractometer is set up to measure the integrated intensity $I_X(\psi)$ under asymmetric conditions, the angle of divergence is fixed at α_0 and W varies because of the changing angle ψ. The appropriate $f(W)$ term corresponds to the value of W given by Equation 7 with $\alpha = \alpha_0$ (typically 1°) and $\omega = (\theta - \psi)$.

The principal objective of this work is to accurately determine the ratio of the integrated intensities, I_A^{111}/I_M^{110}, of the 111 and 110 lines of the austenite and martensite phases that would be obtained if there were no preferred orientation. From the asymmetric diffraction measurements of $I_X(\psi)$ and $f(W)$ for each phase X, it is possible to determine the texture function $\Gamma_X(\psi) = P_X(\psi)I_X^{hkl}$ for each phase over a range of ψ angles using Equation 6,

$$\Gamma_X(\psi) = P_X(\psi)I_X^{111} = \frac{I_X(\psi)}{f(W_X)(1 + \tan\psi \cot\theta_X)} \quad (9)$$

In specimens with random crystallites the orientation distribution term $P_X(\psi) = 1$ at all ψ so that $\Gamma_X(\psi) = I_X^{hkl}$. In addition, all planes in the $\{hkl\}$ family contribute to the intensity term $\Gamma_X(\psi)$. When the crystallites are very strongly oriented the integrated intensity $\Gamma_X(\psi)$ at $\psi = 0^\circ$ is enhanced and $P_X(\psi) \gg 1$ at $\psi = 0^\circ$. However, the orientation function $P_X(\psi)$ decreases to zero very rapidly within a few degrees.

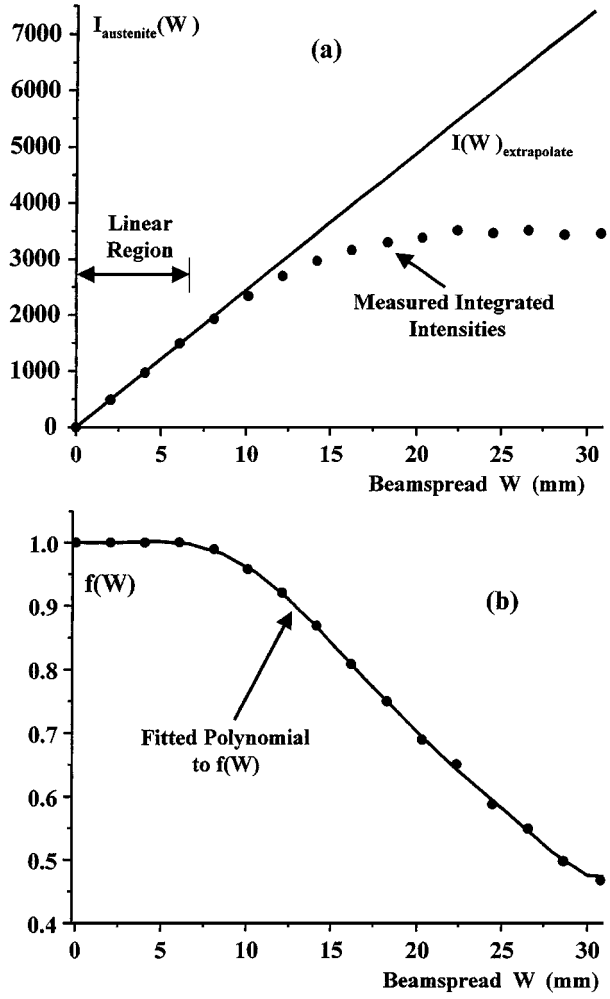

Figure 6 (a) Integrated intensity $I(W)$ measured at different levels of the beamspread W of the incident beam on one of the orthodontic wire samples. The beamspread was varied by increasing the divergence angle α of the beam, (b) Measured correction factor $f(W)$ for finite specimen size when the spread of the incident beam is W.

To convert the results for a strongly oriented crystal to the equivalent random integrated intensity I_X^{hkl}, it is necessary to determine the average of $\Gamma_X(\psi)$ over all directions in space [9]. Unlike the random crystallite case, only one member of the $\{hkl\}$ family is contributing to the diffraction at $\psi = 0^\circ$ in a strongly oriented material and the result of averaging is I_X^{hkl}/m_{hkl}. As all the diffraction measurements are carried out with the specimen spinning in its own plane, the measured $\Gamma_X(\psi)$ values already represent an average value at a fixed ψ over the longitudinal coordinate ϕ around the polar axis $\psi = 0$. The mean value of $\Gamma_X(\psi)$ over the surface of a sphere is therefore defined by the equation,

$$\frac{1}{4\pi}\int_0^{\pi} 2\pi \sin\psi\ \Gamma_X(\psi)\,\mathrm{d}\psi = \frac{I_X^{hkl}}{m_{hkl}} \qquad (10)$$

In the orthodontic wires investigated here the texture is not always strong enough for the function $\Gamma_X(\psi)$ to decay rapidly to zero and other planes in the $\{hkl\}$ family contribute a small amount to the integrated intensity over the range of measurement in ψ. In this case the observed function $\Gamma_X(\psi)$ is a sum of Γ functions each representing a different sub-group of hkl planes

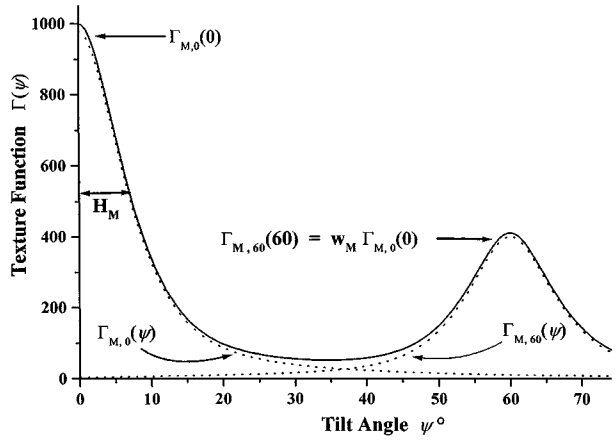

Figure 7 An illustration of the function $\Gamma_M(\psi)$ for a martensite phase showing it as a sum of the texture function $\Gamma_{M,0}(\psi)$ for the 110 planes, and $\Gamma_{M,60}(\psi)$ for the distribution of the (101), (011), (01$\bar{1}$) and (10$\bar{1}$) planes centred on $\psi = 60^\circ$.

in the $\{hkl\}$ family. For the austenite 111 line between $\psi = 0^\circ$ and 12°, $\Gamma_A(\psi)$ is represented as the sum of two functions, i.e.

$$\Gamma_A(\psi) = \Gamma_{A,0}(\psi) + \Gamma_{A,70.5}(\psi) \qquad (11a)$$

where $\Gamma_{A,0}(\psi)$ represents the distribution of the (111) planes centred about $\psi = 0^\circ$, and $\Gamma_{A,70.5}(\psi)$ represents the distribution of the (11$\bar{1}$), (111) and (1$\bar{1}$1) planes centred about $\psi = 70.5^\circ$. Although there are also distributions about $\psi = 109.5^\circ$ and 180° representing other members of the {111} family, these can be neglected in the present case as their contributions at $\psi \leq 12^\circ$ are very small. An illustration of $\Gamma_A(\psi)$ and the contributions of the component functions $\Gamma_{A,0}(\psi)$ and $\Gamma_{A,70.5}(\psi)$ corresponding to the present samples is given in Fig. 7. Similarly, for the martensite 110 line, $\Gamma_M(\psi)$ is represented as the sum, i.e.

$$\Gamma_M(\psi) = \Gamma_{M,0}(\psi) + \Gamma_{M,60}(\psi) \qquad (11b)$$

where $\Gamma_{M,0}(\psi)$ represents the distribution of (110) planes and $\Gamma_{M,60}(\psi)$ represents the distribution of the (101), (011), (01$\bar{1}$) and (10$\bar{1}$) planes.

Under these circumstances, the appropriate function for calculating I_X^{hkl}/m_{hkl} through Equation 10 is $\Gamma_{X,0}(\psi)$ rather than $\Gamma_M(\psi)$. The question therefore is, how can $\Gamma_{X,0}(\psi)$ be extracted from the experimental results $\Gamma_X(\psi)$? In the present results, the dominant contributions to $\Gamma_M(\psi)$ and $\Gamma_A(\psi)$ are $\Gamma_{M,0}(\psi)$ and $\Gamma_{A,0}(\psi)$, respectively, and the higher terms, $\Gamma_{M,60}(\psi)$ and $\Gamma_{A,70.5}(\psi)$, behave as a "background contribution" which typically contribute <2% of the measured $\Gamma_M(\psi)$ or $\Gamma_A(\psi)$ values (see Fig. 7). As a first approximation therefore, it can be assumed that over the fitted range $0^\circ \leq \psi \leq 12^\circ$,

$$\Gamma_M(\psi) \approx \Gamma_{M,0}(\psi)$$

and

$$\Gamma_A(\psi) \approx \Gamma_{A,0}(\psi) \qquad (12)$$

In the examples discussed in this paper the error introduced into the measured volume fraction of martensite V_M by neglecting the higher order terms in $\Gamma_X(\psi)$ is no more than ~2%. Further discussion on the magnitude of this systematic error is given later.

In practice the procedure adopted to determine V_M is to first fit the texture functions $\Gamma_A(\psi)$ and $\Gamma_M(\psi)$ over the measured range in ψ. Pseudo-Voigt functions are used here as these fit well with a shape factor γ between 67% and 100% Lorentzian [12]. The fitted functions are then calculated at 0.1° steps over the range $\psi = 0$ to 180°, weighted by sin ψ, before calculating the numerical integral Ω_X(X = M or A) given by,

$$\Omega_X = \int_0^{180} \sin\psi \Gamma_X(\psi)\, d\psi \tag{13}$$

The full expression used to determine the volume fraction V_M of martensite when Equation 3 is expressed in terms of measured and calculated parameters becomes,

$$\frac{\Omega_M}{\Omega_A} = \frac{V_M}{1 - V_M} \frac{K_M^{hkl}}{K_A^{HKL}} \tag{14}$$

The fitting and numerical integration associated with the above analysis is usually done using the numerical analysis and graphics software package ORIGIN 5.0.

In the present samples the preferred orientation is relatively strong and the texture widths H_A and H_M, as defined in Fig. 7, are all within the band 5° to 13°. For this degree of preferred orientation the overlap between the component functions $\Gamma_{M,0}(\psi)$ and $\Gamma_{M,60}(\psi)$, and between $\Gamma_{A,0}(\psi)$ and $\Gamma_{A,70.5}(\psi)$, is small but not negligible. The basis of the iterative correction procedure developed for compensating for the overlap assumes that the two component functions within any measured $\Gamma_X(\psi)$ have essentially the same shape. but different total areas, so that

$$\Gamma_{A,70.5}(\psi) = w_A \Gamma_{A,0}(\psi - 70.5)$$

and

$$\Gamma_{M,60}(\psi) = w_M \Gamma_{M,0}(\psi - 60) \tag{15}$$

where w_A and w_M are the relative weights of the component peaks (see Fig. 7). This assumption is essentially stating that if the distribution of the (110) planes in the martensite phase around around $\psi = 0°$ is ±10°, then the distribution of the (101), (011), (01$\bar{1}$) and (10$\bar{1}$) planes about $\psi = 60°$ will also be ≈±10°. On this basis the measured $\Gamma_X(\psi)$ terms can be expressed as,

$$\Gamma_A(\psi) = \Gamma_{A,0}(\psi) + w_A \Gamma_{A,0}(\psi - 70.5)$$

and

$$\Gamma_M(\psi) = \Gamma_{M,0}(\psi) + w_M \Gamma_{M,0}(\psi - 60) \tag{16}$$

To develop an overlap correction it is necessary to know the relative weights w_A and w_M. These can be estimated on the basis that three planes contribute to w_A $\Gamma_{A,0}(\psi - 70.5)$ so that when averaged over the surface of a sphere this function will be three times that of the average value of $\Gamma_{A,0}(\psi)$. For the equivalent martensite functions, the equivalent ratio is four to one. Under the conditions appropriate for the present sample, the weighting term w_X (X = A or M) can be reduced from the expression,

$$w_X \cong \frac{M_X}{2 \sin\psi_0} \frac{\int_0^{180} \Gamma_{X,0}(\psi) \sin\psi\, d\psi}{\int_0^{180} \Gamma_{X,0}(\psi) \cos\psi\, d\psi} \tag{17}$$

where $M_X = 3$ or 4 and, $\psi_0 = 70.5°$ or 60° for austenite and martensite, respectively. In the execution of this correction procedure w_X was first estimated by letting $\Gamma_{X,0}(\psi)$ = fitted function $\Gamma_X(\psi)$ in Equation 17. The measured function $\Gamma_X(\psi)$ was then fitted using the model represented by Equation 16 to obtain a new fitted form for $\Gamma_{X,0}(\psi)$. An updated value for w_X can then be obtained using Equation 17 and further iterations carried out to converge on a more accurate form for $\Gamma_X(\psi)$. This was unecessary for the present samples as one iteration was sufficient to obtain an accurate correction.

3. Results and analysis

The texture functions $\Gamma_M(\psi)$ and $\Gamma_A(\psi)$ obtained for the four different wires over the range $\psi = 0°$ to 12° are shown in Fig. 8. This figure also shows the fitted curves $\Gamma_M(\psi)$ and $\Gamma_A(\psi)$ from which the terms Ω_A and Ω_M were determined. The results of the fitting are given in Table I along with the calculated volume fraction V_M of martensite in each wire and the breadths, H_M and H_A, of the functions $\Gamma_M(\psi)$ and $\Gamma_A(\psi)$. A number of different results for V_M are presented, which are discussed in more detail later, comparing the present method with the results obtained if no preferred orientation correction is applied. The terms H_M and H_A reflect the degree of texture in the particular phase and represent the values of ψ at which the fitted texture function $\Gamma_{X,0}(\psi)$ decreases to 50% of its initial value at $\psi = 0°$. All the uncertainties quoted in Table I reflect the precision of the fitting procedure. The atomic scattering factors and associated dispersion corrections used to determine the structure factors for calculating V_M from Equation 14, were obtained from the International Tables for Crystallography Volume C [15]. In the calculation of the structure factors it was assumed that the alloying elements in the wires were substitutionally disordered so that,

$$F_{\text{austenite}} = 4 f \exp(-B_A \sin^2\theta/\lambda^2)$$

and

$$F_{\text{martensite}} = 2 f \exp(-B_M \sin^2\theta/\lambda^2)$$

where $f = 0.700 f_{Fe} + 0.181 f_{Cr} + 0.078 f_{Ni} + 0.014 f_{Mn} + 0.027 f_{Si}$. It was assumed that temperature parameters $B_A = B_M$ and that these values will be ≈0.35 Å^2, the same as Fe at room temperature [16]. The

TABLE I Results obtained after fitting the measured texture function $\Gamma_M(\psi)$ and $\Gamma_A(\psi)$ for each of the four wires. The terms H_M and H_A are a measure of the preferred orientation and represent the ψ angles at which the fitted functions $\Gamma_{M,0}(\psi)/\Gamma_{M,0}(0)$ and $\Gamma_{A,0}(\psi)/\Gamma_M(0) = 0.5$. The three columns labelled V_M are the volume fraction of martensite obtained from the present data, (a) using the present orientation correction assuming $\Gamma_X(\psi) = \Gamma_{X,0}(\psi)$, (b) using the present orientation correction but compensating for overlap between $\Gamma_{A,0}(\psi)$ and $\Gamma_{A,70.5}(\psi)$ and, between $\Gamma_{M,0}(\psi)$ and $\Gamma_{M,60}(\psi)$, (c) using the integrated intensities measured at $\psi = 0^\circ$ and the intensity equation for randomly oriented crystals (Equation 3). The numbers in brackets are the uncertainties that propagate from the uncertainties from fitting the observed texture functions $\Gamma_M(\psi)$ and $\Gamma_A(\psi)$

Wire type	$H_M{}^\circ$	$H_A{}^\circ$	(a) V_M Orientation Correction (No Overlap Correction)	(b) V_M Orientation Correction (+ Overlap Correction)	(c) V_M No Orientation Correction (Random Xtal)
W (1.62 mm)	12.9 (3)	6.8 (2)	0.58 (5)	0.56 (5)	0.25 (1)
W (0.52 mm)	7.1 (2)	6.3 (2)	0.75 (3)	0.74 (3)	0.65 (2)
D (2.18 mm)	12.3 (3)	6.9 (1)	0.72 (3)	0.70 (3)	0.35 (1)
D (0.88 mm)	10.6 (2)	5.7 (2)	0.83 (6)	0.82 (6)	0.47 (2)

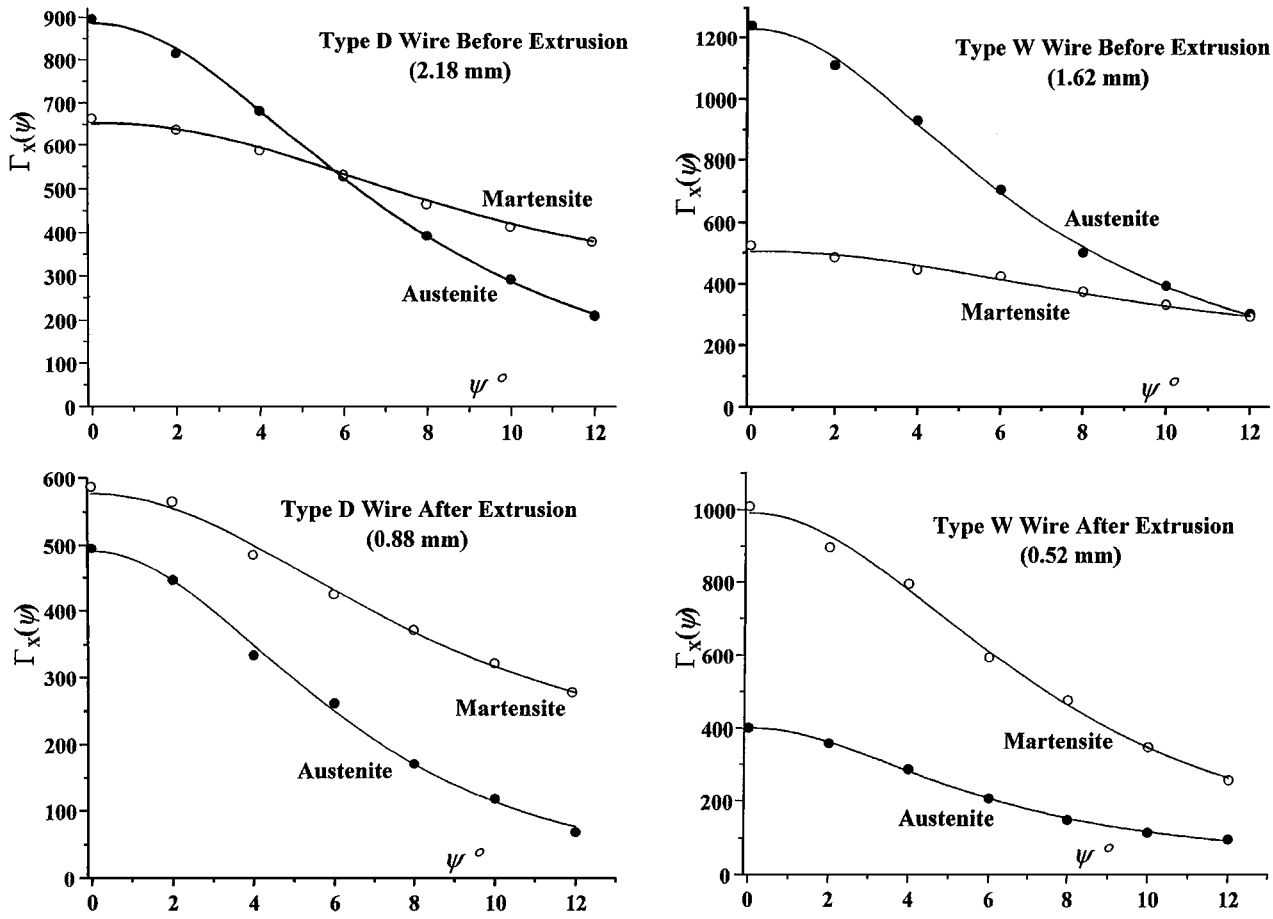

Figure 8 The measured and fitted textures functions, $\Gamma_M(\psi)$ and $\Gamma_A(\psi)$, for each of the four orthodontic wires.

lattice parameters used for calculating the cell volume, $a_{aust} = 3.586$ Å and $a_{mart} = 2.871$ Å, were measured directly from the XRD pattern. As the 111 austenite and 110 martensite lines are $<1^\circ$ 2θ apart, any error in the choice of B parameter or the composition will only have a small effect on the volume fraction V_M determined through Equation 14 as this equation contains the ratio F_M/F_A which $\approx$0.5 irrespective of the temperature parameter B or the alloy composition.

In all the wires the preferred orientation of the austenite phase is stronger than the martensite phase. The width H_A of the austenite phase is consistently between 5.7° and 6.9°, and the extrusion process only increases the texture by a relatively small amount. The texture of the martensite phase is less pronounced than the austenite phase and, with the exception of the finer type *W* wire, $H_M - H_A \geq 5^\circ$. This difference is probably the result of the orientation change that occurs during the austenite-martensite transformation. The actual effect of the extrusion process on the martensite orientation is quite different for the two wires. In the Type *W* wire, in particular, the orientation width H_M decreases by almost 6° on extrusion where as the change in the type *D* wire is $\sim$1.7° and only slightly larger than the change for the austenite phase in this wire.

The fact that the degree of texture in the martensite and austenite is quite different for three of wires is the main factor that makes correction for preferred

orientation very necessary. Column (b) of the results for V_M in Table I which is corrected for both preferred orientation and overlap is the most accurate of the three sets. The results for V_M, labelled "random crystals" (i.e. column (c)) with no orientation correction, were obtained by substituting the integrated intensities for martensite and austenite at $\psi = 0$ into the conventional quantitative analysis equation represented by Equation 3. When the degree of texture of the two phases is similar, as is almost the case for the finer Type *W* wire, the volume fraction V_M obtained by assuming no preferred orientation will be similar to the result obtained after correction for preferred orientation. Under these circumstances the preferred orientation correction terms for the austenite and martensite tend to cancel each other. In three of the wires considered here, the texture of the austenite phase is much stronger than martensite, and the preferred orientation correction terms are different for each phase. As a consequence, application of the "random crystal" intensity equation severely under-estimates the martensite content by up to 50%. To within a 10% margin, the volume fraction obtained after correction for preferred orientation, $V_M^{\text{corrected}}$, is related to the volume fraction obtained from the "random crystal" intensity equation, V_M^{random}, as,

$$V_M^{\text{corrected}} \approx 1.05 \frac{H_M}{H_A} V_M^{\text{random}} \tag{14}$$

Unfortunately, it was not possible to compare the present results for V_M with those using other techniques. Both magnetic measurements and transmission electron microscopy (TEM) were carried out on the specimens, but neither technique provided reliable results. TEM images were uniformative because of the fine grain structure of the orthodontic wires and the fact that both phases are twin structures of almost identical appearance. Magnetic measurements on orthodontic wires are difficult to interpret, and measurements carried out on the present wires at another laboratory were clearly inconsistent with the X-ray results. In particular, for one of the specimens shown in Fig. 1, magnetic measurements gave zero martensite content which is clearly in error given the magnitude of the martensite peak.

The uncertainties quoted in Table I for volume fractions V_M of martensite after correction for preferred orientation range from $\pm 4\%$ up to $\pm 8\%$. These uncertainties reflect standard deviations associated with fitting the texture function $\Gamma_X(\psi)$ to determine $\Gamma_{X,0}(\psi)$ and its subsequent extrapolation beyond the measured range to calculate the integral terms $\Omega_X = \int_0^{180} \sin\psi \Gamma_{X,0}(\psi)\, d\psi$. For the texture widths encountered in the austenite and martensite phases this uncertainty is significantly greater than the correction for overlap between the component functions within each $\Gamma_X(\psi)$ function. To obtain an accurate estimate of the integral Ω_X it is of central importance to be able to predict the shape of the tail of $\Gamma_{X,0}(\psi)$ with reasonable accuracy because of the weighting introduced by the "$\sin\psi$" within the integrand of Ω_X. In the present data, the extrapolated austenite functions $\Gamma_{A,0}(\psi)$ are more reliable than the corresponding martensite functions $\Gamma_{M,0}(\psi)$. Although both sets of fitted functions extend beyond measurement limit of ψ, the texture widths H_M of all but one of the martensite results are also larger than 12°, the maximum measured ψ. This makes the extrapolation of $\Gamma_{M,0}(\psi)$ beyond 12° very sensitive to the accuracy of both the fitted texture width H_M and the pseudo-Voigt parameter γ_M which describes the degree of Lorenzian character of $\Gamma_{M,0}(\psi)$. At one extreme, when the fitted function is close to Lorentzian (i.e. $\gamma_M \approx 1$) $\Gamma_{M,0}(\psi)$ needs to be extrapolated to $\psi \approx 6H_M$ before decaying to the noise level. Conversely, when the texture function is Gaussian shaped (i.e. $\gamma_M \approx 0$) the function $\Gamma_{M,0}(\psi)$ decays very rapidly within $\psi \approx 3H_M$ and the uncertainty of the extrapolated function is less.

The accuracy of the results presented here, would have been better had Cr K_α radiation been available ($\lambda = 2.29$ Å). At this wavelength the 111 and 110 lines shift from $2\theta \approx 45^\circ$ up to $\approx 67^\circ$ thereby increasing the upper limit of ψ from 12° up to $\sim 25^\circ$. The only drawback is a larger overlap correction because of the greater contribution of the higher order components $\Gamma_{M,60}(\psi)$ and $\Gamma_{A,70.5}(\psi)$ in the range of measurement. To obtain an accuracy $\approx 5\%$ or less for the volume fraction V_M using the method proposed here, it is recommended that the texture widths, H_M and H_A, be less than 10° and that the measured ψ range be at least twice the largest H_X value. As the texture widths become larger and the measurement range become smaller, the uncertainty in the extrapolated texture functions grows along with the uncertainty in V_M.

Acknowledgements

Ms Ying Ma-Sorrell wishes to thank the Australian Government for the support provided for this work by way of an Australian Postgraduate Award Scholarship.

References

1. S. FRIEL, *Int. J. Orthod.* **20** (1934) 972.
2. R. C. THUROW, "Edgewise Orthodontics" 3rd ed. (CV Mosby Company, St Louis, 1972) p. 38.
3. A. J. GOLDBERG, R. VANDERBY JR. and C. J. BURSTONE, *J. Dent. Res.* **56** (1977) 1227.
4. W. A. BRANTLEY, W. S. AUGAT, C. L. MYERS and R. V. WINDERS, *ibid.* **57**(1978) 609.
5. D. A. PORTER and K. E. EASTERLING, "Phase Transformations in Metals and Alloys" 2nd ed., (Chapman & Hall, London, 1992) p. 382.
6. P. L. MANGONON JR. and G. THOMAS, *Metallurgical Transactions* **1** (1970) 1577.
7. R. P. REED and C. J. GUNTNER, *Trans. Metal Soc. AIME* **230** (1964) 1713.
8. Z. YAJIMA, Y. KISHI and Y. HIROSE, *Adv. in X-ray Analysis* **39** (1997) 481.
9. C. S. BARRETT and T. B. MASSALSKI, "Structure of Metals" 3rd ed., (Mc Graw-Hill, New York, 1966) p. 193.
10. H. P. KLUG and L. E. ALEXANDER, "X-ray Diffraction Procedures" 2nd ed., (Wiley, New York, 1974) p. 709.
11. M. D. VAUDIN, M. W. RUPICH, M. JOWETT, G. N. RILEY and J. F. BINGERT, *J. Mat. Res.* **13**(1998) 2910.
12. R. J. YOUNG, "The Rietveld Method" (International Union of Crystallography & Oxford University Press, Oxford, 1993) p. 9.
13. R. W. CHEARY and A. A. COELHO, *J .Appl. Cryst.* **25**(1992) 109.

14. R. W. CHEARY and A. A. COELHO, Program XFIT deposited in CCP14 Powder Diffraction Library, UK Engineering and Physical Sciences Research Council, Daresbury Laboratory, Warrington, UK. Internet address: *www.ccp14.ac.uk*.
15. "International Tables for Crystallography, Vol. C" (Kynoch Press, Birmingham, 1990).
16. "International Tables for Crystallography, Vol. 3" (Kynoch Press, Birmingham, 1962).

Received 12 May
and accepted 19 August 1999